

A high-performance Li-ion anode from direct deposition of Si nanoparticles

Xu, Yaolin; Swaans, Ellie; Chen, Sibó; Basak, Shibabrata; Harks, Peter-Paul; Peng, Bo; Zandbergen, Henny W.; Borsa, Dana M.; Mulder, Fokko M.

DOI

[10.1016/j.nanoen.2017.06.011](https://doi.org/10.1016/j.nanoen.2017.06.011)

Publication date

2017

Document Version

Final published version

Published in

Nano Energy

Citation (APA)

Xu, Y., Swaans, E., Chen, S., Basak, S., Harks, P.-P., Peng, B., Zandbergen, H. W., Borsa, D. M., & Mulder, F. M. (2017). A high-performance Li-ion anode from direct deposition of Si nanoparticles. *Nano Energy*, 38, 477-485. <https://doi.org/10.1016/j.nanoen.2017.06.011>

Important note

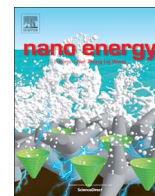
To cite this publication, please use the final published version (if applicable).
Please check the document version above.

Copyright

Other than for strictly personal use, it is not permitted to download, forward or distribute the text or part of it, without the consent of the author(s) and/or copyright holder(s), unless the work is under an open content license such as Creative Commons.

Takedown policy

Please contact us and provide details if you believe this document breaches copyrights.
We will remove access to the work immediately and investigate your claim.



Full paper

A high-performance Li-ion anode from direct deposition of Si nanoparticles

Yaolin Xu^a, Ellie Swaans^b, Sibon Chen^a, Shibabrata Basak^c, Peter Paul R. M. L. Harks^a, Bo Peng^{a,d}, Henny W. Zandbergen^c, Dana M. Borsa^b, Fokko M. Mulder^{a,*}



^a Materials for Energy Conversion and Storage (MECS), Department of Chemical Engineering, Faculty of Applied Science, Delft University of Technology, Van der Maasweg 9, 2629 HZ Delft, The Netherlands

^b Meyer Burger (Netherlands) B.V., Luchthavenweg 10, 5657 EB Eindhoven, The Netherlands

^c Kavli Institute of Nanoscience Delft, Department of Quantum Nanoscience, Delft University of Technology, Lorentzweg 1, 2628 CJ Delft, The Netherlands

^d Department of Physics, Renmin University of China, No. 59 Zhongguancun Street, Haidian District, 100872 Beijing, China

ARTICLE INFO

Keywords:

Li ion battery
Si nanoparticles
Direct deposition
One-off SEI formation

ABSTRACT

Nanostructured silicon has been intensively investigated as a high capacity Li-ion battery anode. However, the commercial introduction still requires advances in the scalable synthesis of sophisticated Si nanomaterials and electrodes. Moreover, the electrode degradation due to volume changes upon de-/lithiation, low areal electrode capacity, and application of large amounts of advanced conductive additives are some of the challenging aspects. Here we report a Si electrode, prepared from direct deposition of Si nanoparticles on a current collector without any binder or conducting additives, that addresses all of the above issues. It exhibits an excellent cycling stability and a high capacity retention taking advantages of what appears to be a locally protective, yolk-shell reminiscent, solid electrolyte interphase (SEI) formation. Cycling an electrode with a Si nanoparticle loading of 2.2 mg cm^{-2} achieved an unrivalled areal capacity retention, specifically, up to 4.2 mAh cm^{-2} and $\sim 1.5 \text{ mAh cm}^{-2}$ at 0.8 mA cm^{-2} and 1.6 mA cm^{-2} , respectively.

1. Introduction

Energy storage is one of the key issues of modern society. The development of Li-ion battery based energy storage devices is flourishing, in an effort to meet the increasing power demand of a diverse range of applications, such as electrical vehicles and widely used portable electronics [1–5]. Si based anode materials have been extensively studied for Li ion batteries mostly due to the unparalleled theoretical capacity of Si (4200 mAh g^{-1} for $\text{Li}_{4.4}\text{Si}$). However, the huge volume change and its resulting electrode pulverization upon Li uptake leads to electrical conduction loss and rapid capacity degradation, which has severely reduced its promise for practical applications [6–9]. Research has been focusing on various kinds of nanostructured Si materials to resolve the different aspects leading to capacity loss, and to achieve stable cycling performance [10–12]. Current studies mostly synthesize sophisticated nanostructured Si, including nanowires [13,14], nanotubes [15,16], nanospheres in a flexible matrix or 3D architecture [17,18], etc., or apply protective coatings [19,20] to prevent electrode pulverization and to provide continuous electronic and ionic conduction pathways during cycling. However, these synthetic approaches on a lab scale appear to have poor scalability and therefore until now limit large scale commercial viability. Moreover,

methods that do use potentially more scalable methods involve large amounts of additional relatively costly nanoscale carbonaceous conducting networks (graphene [21], carbon nanotube [22], carbon nanofiber [23], etc.) and advanced binder materials [24,25], which lowers the cost-effectiveness and overall capacity that is realized.

Another major challenge for Si based anodes is to enhance the areal capacity, which is generally poor owing to the low mass loading of active materials [14–17,26–28]. Progress has been made to increase the mass loading of Si and/or electrode packing density to improve the performance [29–36], but these electrode manufacturing approaches are still hardly industrially viable as they introduce either high cost materials or complicated production processes.

Thus the main challenge for the practical implementation of Si anodes is to develop cost-effective and commercial viable techniques to prepare Si anodes. The technique should be capable of producing Si particles that are nanosized to accommodate volume changes, and that are electronically connected throughout the structure. In addition the technique should have a high production rate and be scalable. When possible advanced carbons and binders in the process should be minimized and further processing for electrode manufacturing should also be eliminated. Progress has been made to realize the scalable synthesis of nanostructured Si anodes [37–40] as well as to produce

* Corresponding author.

E-mail address: F.M.Mulder@tudelft.nl (F.M. Mulder).

<http://dx.doi.org/10.1016/j.nanoen.2017.06.011>

Received 15 March 2017; Received in revised form 5 June 2017; Accepted 6 June 2017

Available online 13 June 2017

2211-2855/© 2017 The Authors. Published by Elsevier Ltd. This is an open access article under the CC BY-NC-ND license (<http://creativecommons.org/licenses/by-nc-nd/4.0/>).

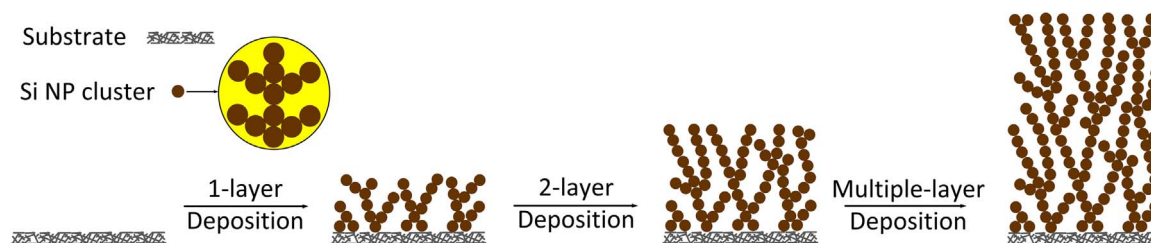


Fig. 1. A schematic of electrode preparation process via direction deposition of Si nanoparticles.

binder-free Si electrodes [41–46].

In this study, a novel but simple and industrially scalable process was developed to synthesize Si anodes. (Fig. 1) In this process silicon nanoparticles (Si NP) are directly deposited on a porous carbon current collector by plasma enhanced chemical vapour deposition (PECVD). The obtained additive- and binder-free electrode can be used as an anode in a Li-ion battery without further processing.

Previous studies on the Si deposition based Li ion anodes consider Si nanowires, nanoscale Si films on 3D substrates, or thin structured Si films [13–16,28,42,47–50]. The novel approach in this work introduces a facile one-step synthesis by direct deposition of Si nanoparticles with at least an order of magnitude higher mass loading of Si compared to the previous studies (max. 5 μm Si layer in previous reports), and without the need for catalysts or other additional 3D nanostructures. The Si electrode in this work exhibits several advantages: (1), CVD based Si deposition is industrially well-developed and scalable due to its present widespread applications in solar cells and electronics. The thickness and porosity of Si NP deposition layers can be monitored and controlled. (2), The plasma aided self-assembly of nanoparticle layers produces hierarchical nano and micro structured Si NP branched structures, which results into sufficient porosity to accommodate the volume expansion during Li ion uptake. (3), The Si nanoparticles appear naturally interconnected, which eliminates the need for binders and conductive additives and thus improves the overall capacity of the electrode and reduces the processing cost. (4), Controlled oxidation on the surface of Si NP is achieved through low pressure O_2 exposure between the plasma deposition cycles. The inactive and solid SiO_x scaffold appears to reinforce the structural integrity of the electrode during cycling. (5), The inter-particle porosities are connected in nanoscale, which provides an express way for electrolyte infiltration and thus good Li ion transport throughout the electrode. Hence high performance can be reached for electrodes with increased thicknesses, enabling high areal capacities with increased Si mass loading. (6), A templating effect [51,52] is introduced by the open porosity of the used carbon substrate. This results in interconnected micron scale porosities allowing electrolyte to enter the Si NP layer, which shortens the diffusion pathway of Li ion towards active materials and thus enables fast Li ion transport within the electrode. (7), The density of this Si NP electrode ($\sim 0.5 \text{ g cm}^{-3}$) may not appear high but this is about 20% of the density of bulk silicon, significantly higher than in other reports where a much smaller fraction of the bulk Si density is reached [15,16,28,47]. The density is however sufficiently low to allow space for the large volume expansion of Si; up to 400% expansion would just fill the total available volume, let alone the space required for the SEI growth.

2. Methods

2.1. Electrode preparation

The Si NP electrodes were prepared via PECVD from silane using an Expanding Thermal Plasma (ETP) source [53,54]. Si NP depositions were performed on a porous carbon sheet (Caplinq) layer by layer and each layer includes 30s' deposition of Si NP. The specific process and conditions for the Si NP deposition are stated in the Supporting

information (SI). The as-synthesized Si NP-C sample was directly applied as the electrode after drying in a vacuum oven for 12 h. For comparison, Si NP deposition was also carried out on a non-porous planar Cu foil (Goodfellow, 12.7 μm) and its morphology before and after de-/lithiation is shown in SI.

2.2. Sample characterization

For the pristine Si NP electrode, Scanning Electron Microscopy (SEM) images were taken using a JEOL JSM 6010 F scanning electron microscope at an accelerating voltage of 5 kV; The high resolution SEM images were acquired using Hitachi S4800 working at 2 kV. For Transmission Electron Microscopy (TEM) measurement Si particles were carefully scraped off from the electrode. Bright field TEM images were acquired using FEI-Tecnaï operating at 200 kV. X-ray diffraction (XRD) patterns were measured with a PANalytical X'Pert Pro PW3040/60 diffractometer with Cu K α radiation operating at 45 kV and 40 mA. Raman spectra on Si NP particles were obtained from a Renishaw InVia Raman spectrophotometer. The wavelength of the laser applied is 785 nm and the laser power is set at 0.2 mW. Thermal Gravimetric Analysis (TGA) was carried out with a Perkin Elmer TGA 7 thermogravimetric analyser. The Si NP sample were scraped from the carbon substrate and heated in a 20% O_2/Ar mixture from room temperature to 1000 $^\circ\text{C}$ followed by a full oxidation at 1000 $^\circ\text{C}$ for 200 min. X-ray photoelectron spectroscopy (XPS) was performed with a K-Alpha XPS System.

All cycled electrodes were washed with diethyl carbonate (DEC) for 3 times to remove soluble electrolyte residuals in the electrode, and were dried in a glove box before the measurement. The SEM images were acquired using Hitachi S4800 with an accelerating voltage of 15 kV. STEM-EDX (Energy Dispersive X-ray spectroscopy) mapping was done at FEI-Titan operating at 300 kV with Oxford instrument EDX system. TEM, XRD and XPS measurement were performed using the same equipment and working conditions as were utilized for pristine samples.

2.3. Electrochemistry

The half-cell employed for the electrochemical measurement was a lab-designed prototype (Fig. S1) which consists of two stainless steel flanges, an O-ring in between the flanges, and a plastic vacuum clamp to hold them together. There is a separate stainless steel plate supported by a metal spring to provide the necessary pressure and mechanical compaction inside the battery. Half-cell Li ion batteries for test were assembled inside an Ar environment glovebox with the O_2 and H_2O levels < 0.1 ppm. A Li metal foil (Aldrich) worked as the counter electrode. A borosilicate glass micro fibre (Whatman) was applied as the separator, and 1 M LiPF_6 dissolved in DEC, ethylene carbonate (EC) and fluoroethylene carbonate (FEC) (1:1:1 in volume) was utilized as the electrolyte.

The galvanostatic electrochemical performance was measured with a MACCOR 4600 battery cycler at room temperature. The cut-off voltages for discharge and charge were 0.005 V and 2 V versus Li/Li^+ , respectively. Cyclic voltammetry was performed with a PGSTAT302N Autolab potentiostat within the same voltage range. Electrochemical

impedance spectroscopy (EIS) measurements were carried out with a PGSTAT302N Autolab within the frequency range of 1 MHz and 0.01 Hz.

2.4. Subtraction of the carbon capacity

Specific capacities of the Si NP reported in this paper were calculated based on the mass of the Si NP layer (excl. the carbon substrate). The capacity of the carbon substrate was determined by measuring the capacity retentions of the carbon paper at a series of current rates and then fitting the capacity data with a logistic function; (Fig. S3) using this function, the capacities of the carbon substrate could be calculated regarding the corresponding current rates applied on carbon. The specific capacities of the Si NP were determined by subtracting the capacity of carbon from that of the Si NP-C electrode. (More details about the subtraction of the capacity contribution from the carbon substrate are described in SI.)

3. Results and discussions

3.1. Electrode manufacturing and characterization

Si NP anodes were synthesized via expanding thermal plasma chemical vapour deposition from silane. Si NP depositions were performed on a planar but porous carbon substrate layer by layer; cooling and air exposure were applied in between. In this study 1–4 layers of Si NP depositions were carried out on the carbon substrates. The as-prepared Si NP-C electrodes are tested in a half cell with a Li metal counter electrode, separator and liquid electrolyte.

Fig. 2 shows the morphology of a 4-layer Si NP deposition on the

carbon sheet. The thickness of the Si NP layer is around 40 μm (Si NP: $\sim 2 \text{ mg cm}^{-2}$). SEM (Fig. 2a–g) shows that small silicon nanoparticles ($< 20 \text{ nm}$) form clusters with typical sizes of approximately 100 nm scale, and a hierarchically multi-branched porous nanostructure appears throughout the Si NP layers. TEM (Fig. 2h–j) demonstrates that the particles reside as clusters of $\sim 100 \text{ nm}$ scale; while individual particles ($\sim 20 \text{ nm}$) are spherical with a very thin native SiO_x layer on the surface. The oxidation layers are amorphous as only XRD peaks of crystalline Si are observed (Fig. 2k). While the presence of both amorphous and crystalline Si phases is evidenced by Raman spectroscopy (Fig. 2l). EDX elemental mapping performed on the Si NP layer (Fig. S5) shows that the oxygen distribution is uniform throughout the Si NP layers. Individual Si nanoparticles are thus homogeneously oxidized on the surface, which is also consistent with the TEM results. To determine the amount of oxygen present in the sample, TGA (Fig. S6) was applied by heating the Si NP under 20% O_2/Ar gas and fully oxidizing Si into SiO_2 . The result indicates the fraction of Si inside the sample amounts to 46.3 wt % (i.e. Si: $\text{SiO}_2 = 0.65: 0.35$ in mole). Such an amount of SiO_2 is consistent with the observation of a very thin layer (1.6 nm) on a 15 nm diameter Si particle in the high resolution TEM images.

3.2. Electrochemical performance

The electrochemical performance of the Si NP-C electrode was verified by cycling the electrode against a Li metal counter electrode. The electrochemical performance of Si NP-C electrodes has contributions from both Si NP and the carbon substrate. The capacity contribution from the carbon substrate was determined and subtracted from that of the Si NP-C electrode. Details about the capacity

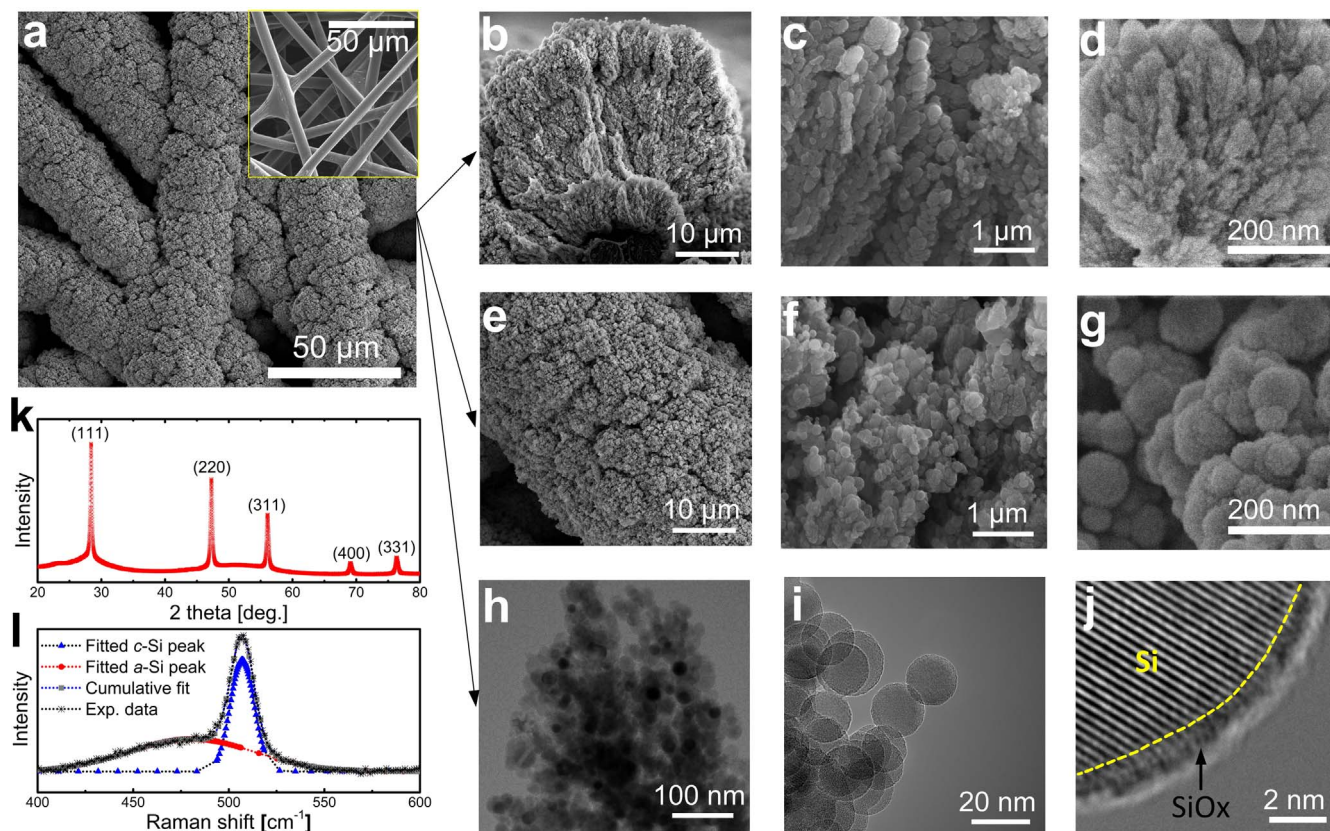


Fig. 2. Morphology of as-synthesized Si NP on a porous C substrate. (a), A SEM image of the Si NP electrode. inset of (a): SEM micrograph of the porous C fibre sheet applied as a substrate for Si deposition. (b) - (d), cross-sectional and (e) - (g), top view SEM micrographs of the nanostructured Si layer imaged at different magnifications. (h) - (j), TEM images of a Si nanoparticle cluster and individual particles as-synthesized from PECVD. (k), XRD patterns of Si nanoparticles as synthesized (the specimen for X-ray diffraction was loose Si nanoparticles scraped from the substrate). (l), Raman spectra of the Si nanoparticles indicating the co-existence of crystalline and amorphous Si.

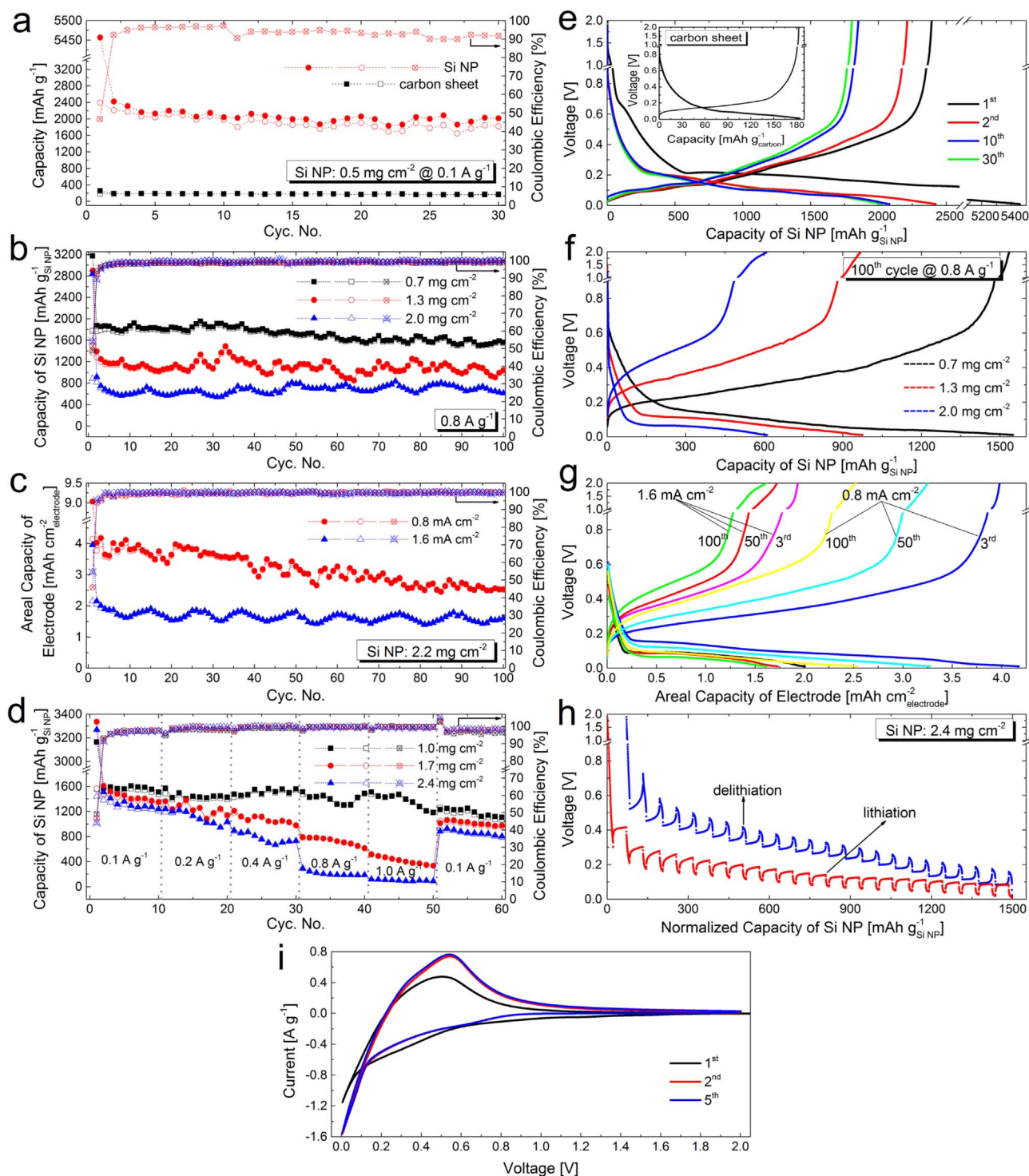


Fig. 3. Electrochemical performance of the Si NP-C electrode for de-/lithiation at room temperature. (a), Capacity retentions and Coulombic efficiencies of Si NP (0.5 mg cm^{-2}) at 0.1 A g^{-1} and the capacity retentions of the carbon substrate cycling with the same measurement program. (b), Electrochemical performance of the Si NP-C electrodes with different mass loadings cycling at 0.8 A g^{-1} . (c), Areal capacity retentions and Coulombic efficiencies of the Si NP-C (2.2 mg cm^{-2}) electrodes cycling at 0.8 and 1.6 mA cm^{-2} . (d), Rate capabilities of Si NP electrodes with different mass loadings. (In Fig. 3a – d, solid symbols: lithiation capacities; open symbols: delithiation capacities; cross-centered open symbols: Coulombic efficiencies.) (e), Voltage profiles of Si NP (0.5 mg cm^{-2}) at 0.1 A g^{-1} . Inset of Fig. (e): voltage profiles of the carbon substrate. (f), Voltage responses of the Si NP-C electrodes with different mass loadings cycling at 0.8 A g^{-1} . (g), Voltage profiles of the Si NP-C (2.2 mg cm^{-2}) electrodes cycling at 0.8 and 1.6 mA cm^{-2} . (h), GITT de-/lithiation of the Si NP-C electrode. GITT was carried out on the thickest Si NP-C electrode (2.4 mg cm^{-2}) following the rate performance test in Fig. (g). Current pulses: 0.1 A g^{-1} for 1 h during charge/discharge; Relaxation for 4 h. (i), Cyclic voltammograms of the Si NP-C electrode (scan rate: 0.5 mV s^{-1}).

subtraction are described in Section 2 and SI. In this paper, all the reported specific capacities are calculated based on the mass of the Si NP layer, including the mass of SiO_2 .

Cycling a Si NP (mass loading of 0.5 mg cm^{-2}) electrode on the carbon substrate at 0.1 A g^{-1} shows a highly stable reversible capacity

(Fig. 3a). A delithiation capacity retention of 1825 mAh g^{-1} is obtained after 30 cycles; Given that the amount of SiO_x accounts for about half of the sample, the specific capacity of Si (excl. SiO_x) would be doubled and therefore be remarkably close to the theoretical capacity assuming SiO_x does not contribute to the reversible capacity.

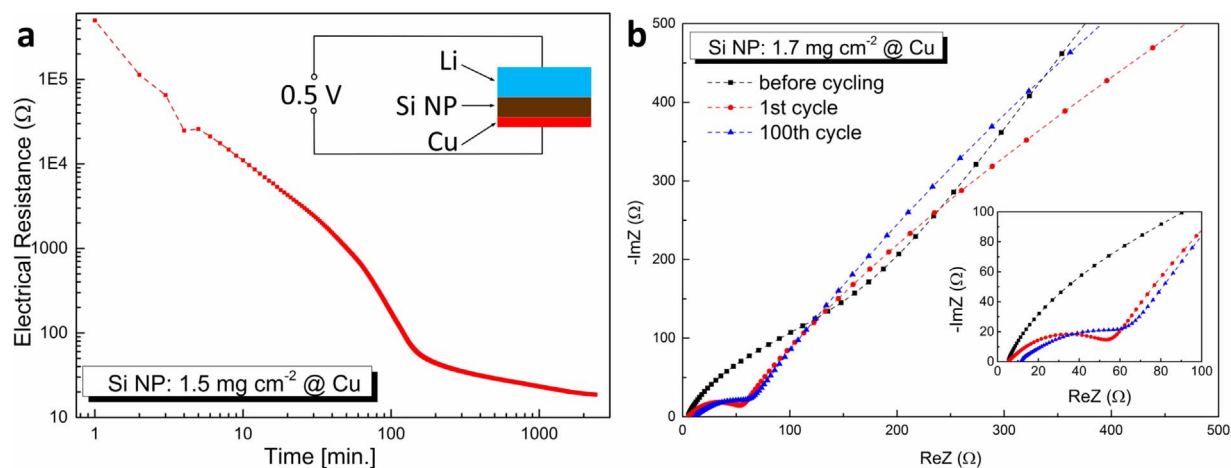


Fig. 4. Impedance measurements. (a), The electronic DC resistance of the Si NP layer during chemical lithiation; inset: experimental set-up of in-situ impedance measurement during chemical lithiation of Si NP. The influence of the Cu substrate, Li foil and cell tester has been subtracted by carrying out a parallel experiment with the same set-up and test conditions but replacing the Si NP-Cu electrode with a blank Cu foil without Si NP. (b), Nyquist plots of the Si NP anode in a half cell with Li metal counter electrode and liquid electrolyte: before cycling and after 1, and after 100 cycles.

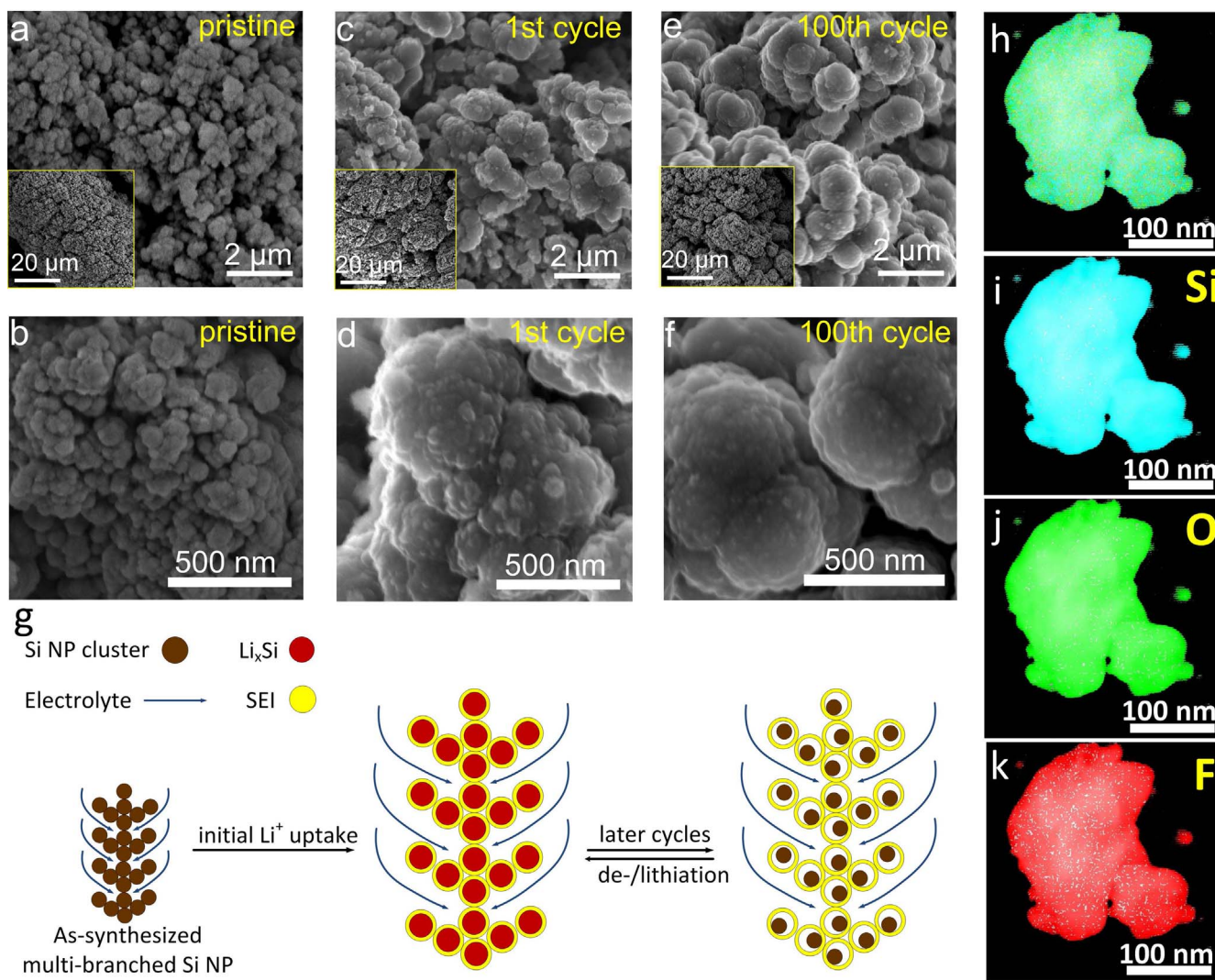


Fig. 5. Morphology of the Si NP electrode at different stages: pristine, 1st cycle and 100th cycle cycling at 0.8 A g^{-1} . (a) - (f), SEM images showing the morphology of Si NP clusters at different stages: (a) - (b), pristine; (c) - (d), SEI shell after 1st cycle; (e) - (f), SEI shell after 100th cycle; (g), A schematic of the morphology change of the hierarchically nanostructured Si NP during de-/lithiation process. (h) - (k), STEM-EDX result: layered image and element mapping of Si, O and F, respectively. The measurements were performed on electrode after 100 de-/lithiation cycles at 0.8 A g^{-1} .

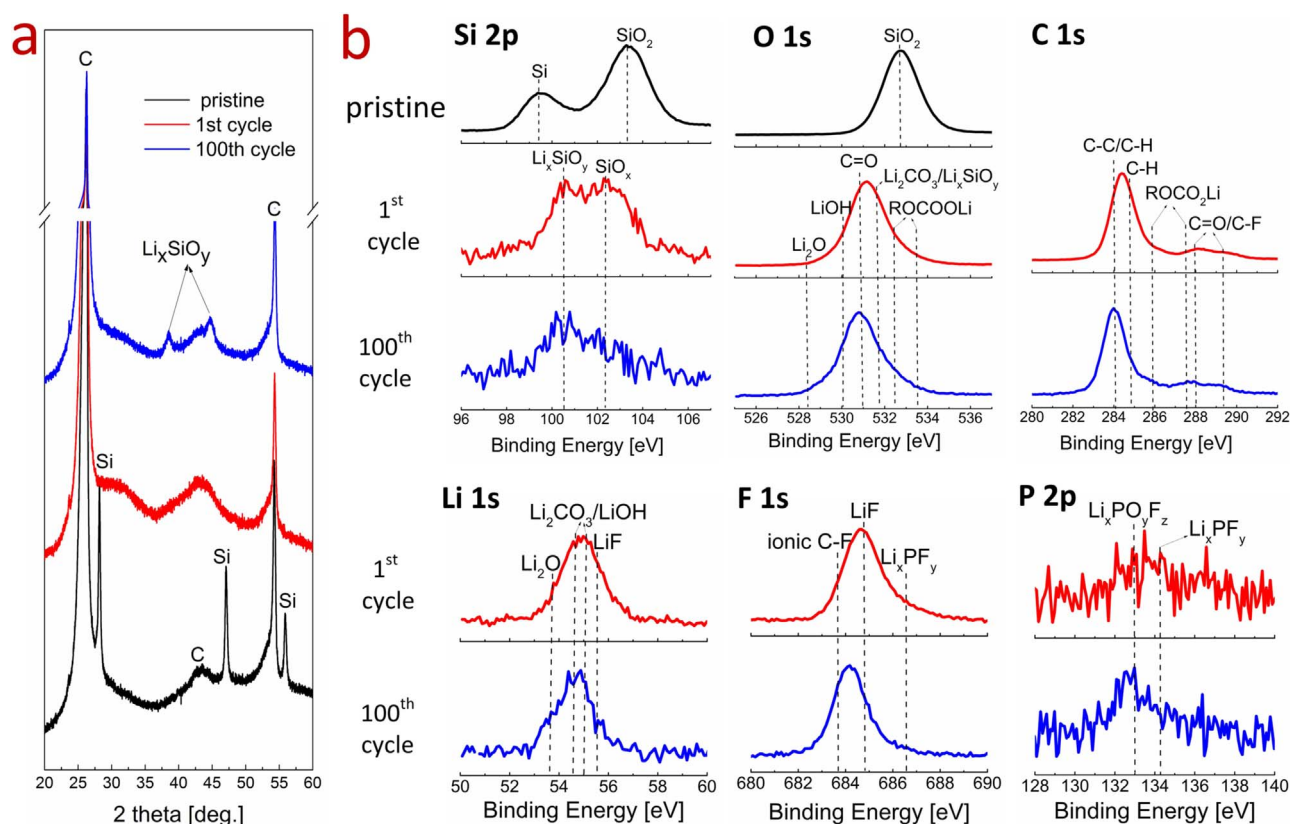


Fig. 6. Characterization on the Si NP electrode at different stages: pristine, 1st cycle and 100th cycle cycling at 0.8 A g^{-1} . (a), XRD patterns of the Si NP electrode. (b), XPS spectra of the Si NP electrode. The electrodes were washed with DEC for 3 times to remove any chemical residuals (mainly LiPF_6) on the electrode and were then dried in glove box to evaporate any organic volatile compounds (mostly DEC) before XPS and XRD measurement.

Fig. 3b demonstrates a remarkable cycling stability over 100 cycles for Si NP-C electrodes with various mass loadings cycling at 0.8 A g^{-1} . The small and periodic capacity fluctuations stem from ambient temperature variations. At this charge rate the achieved capacity of Si NP-C declines with growing Si NP loadings; the capacity reaches around 1600 mAh g^{-1} , 1200 mAh g^{-1} and 800 mAh g^{-1} for electrodes with 0.7 mg cm^{-2} , 1.3 mg cm^{-2} and 2.0 mg cm^{-2} Si NP, respectively. The slight capacity fading along cycling originates from the gradual structural deformation along repetitive dis-/charges.

Cycling at 0.8 mA cm^{-2} the areal capacity for the Si NP-C electrode (Fig. 3c) drops gradually, regardless of the slight swings, from the initial reversible capacity of 4.2 mAh cm^{-2} to 2.5 mAh cm^{-2} after 100 cycles. A greatly promoted cycling stability is observed when the current density is increased to 1.6 mA cm^{-2} which demonstrates an areal capacity retention of about 1.5 mAh cm^{-2} and no apparent capacity degradation after 100 cycles. The improvement of cycleability, when the current rate increases from 0.8 mA cm^{-2} to 1.6 mA cm^{-2} , results from the rapid and incomplete lithiation of Si NP at high current rate and therefore less structural deformation along cycling. The achieved areal capacity is high compared to the recent literature reports on advanced Si based electrodes (Table S2).

Galvanostatic dis-/charge of the Si NP-C electrodes also shows an excellent rate capability. (Fig. 3d) A remarkable rate performance is observed for the Si NP-C electrode with a relative lower mass loading (1.0 mg cm^{-2}). The capacity achieved at 0.1 A g^{-1} reaches $> 1600 \text{ mAh g}^{-1}$; and no apparent capacity degradation occurs when the current rate is increased to higher currents up to 1 A g^{-1} . Increasing the mass loading of Si on carbon sheet slightly reduces capacities. $\sim 1400 \text{ mAh g}^{-1}$ for 1.7 mg cm^{-2} and above 1300 mAh g^{-1} for 2.4 mg cm^{-2} , respectively, have been realized for deep lithiation (i.e. low current densities); The capacity fades with either rising current rates or increases in mass loadings.

Measuring the electrochemical performance of the electrode at different constant temperatures between 10°C and 40°C (Fig. S7), it is observed that a higher temperature leads to a higher initial capacity and a relatively faster degradation. A lower temperature results into a lower capacity retention but a much more stable cycling stability. Moreover, regardless of the capacity retention disparity at different temperatures, no obvious capacity swings can be observed. This reveals that the phenomenon of apparent capacity fluctuations observed in Fig. 3 results from the temperature variations between day and night in the laboratory. It is more pronounced for the electrode with a higher mass loading because the absolute value of the applied current (0.8 A g^{-1}) is higher for a larger mass.

The main de-/lithiation of Si NP occurs at a lower voltage range ($< 0.8 \text{ V}$), which is evidenced by the voltage profiles (Fig. 3e–h) and the cyclic voltammograms (Fig. 3i). A solid electrolyte interphase (SEI) layer is formed, due to the decomposition of the organic electrolyte solvent and reaction with the electrode materials, at a higher voltage plateau (0.7 V , Fig. 3e) during the initial Li ion uptake. Nevertheless, this phenomenon is not observed in the following cycles; instead, later cycles show highly reversible capacities and rather symmetrical voltage profiles for charge and discharge indicating a low overpotential between charge and discharge. Fig. 3f & g demonstrate that the overpotential grows when the mass loading of Si NP is higher and at elevated current rates, which is due to the limited Li ion diffusivity in the Si NP electrode and intrinsic electronic conductivity. However, regardless of the increasing overpotentials, considerable reversible capacity retentions are still achieved.

To study the equilibrium potential the galvanostatic intermittent titration technique (GITT) was applied by pulsing a current of 0.1 A g^{-1} for 1 h and a relaxation period of 4 h after each pulse. Fig. 3h reports that overpotentials during both Li uptake and release decrease with higher lithiation levels.

3.3. Electronic / ionic conductivity

The electronic conductivity of Si can be expected to be greatly enhanced upon trace amounts of Li insertion, leading to even metallically conducting Si [55–57]. This could be an explanation of why an initially poorly conducting electrode that merely consists of Si nanoparticles is capable of fast Li ion uptake and release. For the as-prepared nanostructured electrode, with its packed structure of individual insulating SiO₂ coated particles, the electrical conduction enhancement induced by Li insertion/doping will be of paramount importance. A simple in-situ resistance measurement was performed during chemical lithiation by pressing a Li foil against the Si NP layers; purely in the solid state, without any electrolyte addition. Fig. 4a demonstrates that the DC electrical resistance of the pristine Si NP layer (1.5 mg cm⁻²) is as high as ~ 500 kΩ. Most remarkably the electrical resistance reduces by one order of magnitude within as little as 2 min of all solid chemical lithiation; it further decreases rapidly to < 50 Ω in 2.5 h. The electronic conductivity of the Si NP layer thus increases by about 4 orders of magnitude during solid state lithiation at room temperature, which is comparable to the published results on electrochemical lithiation of a single Si nanowire / thin solid film (100 nm) [56,57]. This finding may illustrate how the Si NP electrode, even without addition of any conducting additives, achieves sufficient electronic conductivity for Li ion insertion and extraction. The presence of SiO₂ apparently has no large detrimental effect on the DC conductivity.

Furthermore, EIS was performed to investigate the ionic conductivity of the Si NP anode in a half cell with a Li counter electrode and liquid electrolyte. Nyquist plots (Fig. 4b) of the Si NP anode demonstrate semicircles in the high frequency region corresponding to the interface resistance of the Si NP anode related to the SEI layer and charge transfer resistance of Li ions. Linear tails in the low frequency range are related to the long range Li-ion diffusion in the electrode [58,59]. It is observed that before cycling, the charge transfer resistance is large (> 300 Ω) as no electrochemical reaction has happened and a large barrier for Li ion diffusion exists. After the first cycle it decreased significantly to around 70 Ω. After dis-/charge for 100 cycles at 0.8 A g⁻¹, the interface resistance increases only slightly, indicating that there is no apparent change in the transfer resistance of Li-ions from and into the Si NP electrode. This indicates that the composition as well as structure of the electrode has been retained after the first cycle and essentially stays intact during cycling.

3.4. One-off in-situ uniform SEI formation

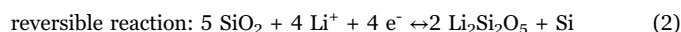
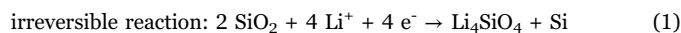
SEI formation is commonly believed to be a crucial disadvantage for nanostructured Si anode materials since repetitive cracking of SEI layers due to the large volume expansion and contraction of the electrode and continuous formation of new SEI ceaselessly reduces available active material, leading to a rapid capacity degradation [4,6,11,60]. However, in this article the SEI layer turns out to behave differently and is even beneficial for the cycling stability.

FEC addition into the electrolyte has been proved to be advantageous as it creates a compact and stable LiF-dominant SEI layer that limits the further formation of SEI [61–63]. Moreover, it is anticipated that a SEI layer will form on the exposed surface of the nano-porous electrode layer of individual particles during the 1st Li ion uptake. Electron microscopy in Fig. 5a–f shows that, regardless of the initial growth of cluster size, the SEI covered Si NP clusters after 100 cycles appear to remain the same typical size as after the 1st cycle. The same is true for the micro-structure of the electrode. Apparently, after the rigid protective SEI is formed, it largely stays intact during later cycles without apparent loss of coherence. There may be a little additional growth, which is consistent with the EIS analysis in Fig. 4b. The rationale for the cycling stability may be that now the volume change of individual particles is accommodated by the space available between

individual particles and their SEI. In this way the contact throughout the electrode is not destroyed during cycling, as illustrated in Fig. 5g. This one-off SEI formation with the remaining coherence throughout the nanoparticle strands is of remarkable advantage. Specifically the local SEI surrounding the particles apparently has outstanding elasticity and mechanical strength, which protects the electrode. It therefore prevents further SEI formation while it also provides ionic conduction.

Furthermore, the SEI layer growth is also investigated by EDX element mapping of F and O (mostly from LiF, Li₂CO₃, and Li-Si-O (see below) in the SEI layer). Fig. 5j & k shows that F and O appear more concentrated in the shell of the Si NP cluster, which may be indicative of its yolk-shell configuration on the scale of the clusters (~ 100 nm). The SEI thus surrounds the clusters of NP, rather than the individual NP. On the larger scale of the entire electrode (10 μm scale) Fig. S9 shows that F and O distribute evenly throughout the electrode indicating a uniform SEI growth throughout the Si NP layer. The resulting morphology of a spontaneous SEI layer around the Si-NP clusters, extending throughout the electrode without breaking the electronic contacts between the clusters apparently exhibits high resistance against stresses caused by the Si volume expansion and contraction of individual particles, therefore it ensures the structural integrity of the Si NP layer and hence supports the cycling stability. In addition it may be deduced from the electrochemical performance that the entire SEI formation takes place only in the first cycles and thus provides a stabilised electrode morphology afterwards.

XRD patterns (Fig. 6a) indicate that crystalline Si is observed in pristine Si NP, and that it has been totally amorphized after the first cycle. Li_xSiO_y compounds can be identified from the XRD spectra after dis-/charge for 100 cycles. Irreversible formation of Li_xSiO_y (mostly Li₄SiO₄, reaction (1)) is commonly recognized for Si/SiO_x based materials; whereas reversible Li₂Si₂O₅ formation (reaction (2)) may also be present [64–66].



The Si 2p XPS spectra (Fig. 6b) of the electrode demonstrate that pristine Si NP consists of Si (99.4 eV) and SiO₂ (103.3 eV). The peak from SiO₂ dominates since XPS is surface sensitive (~ few nm). Upon initial dis-/charge SiO₂ has been partially reduced to SiO_x (~ 102.4 eV); the production of Li_xSiO_y (~ 100.5 eV) is also evident according to reactions (1) and (2); The peak of Si is almost invisible under XPS due to the coverage of the SEI. After 100 cycles, the Si 2p spectrum is dominated by Li_xSiO_y due to the further consumption of SiO_x and formation of Li_xSiO_y (mainly in SEI).

The XPS spectra after 1st cycle indicate that the SEI layer is composed of a series of substances, such as LiF, Li₂CO₃, Li_xSiO_y, and ROCOOLi, etc., which are produced upon the decomposition of organic electrolyte and the following reactions with Si NP. The commonly recognized LiF is evidenced from the dominating peak at 684.8 eV in the F 1s spectrum and the one at 55.5 eV in the Li 1s spectrum. Meanwhile, Li_xPF_y and Li_xPO_yF_z are also observed, which originate from the decomposition of LiPF₆ in the electrolyte.

Comparing the XPS spectra after 100 cycles and after the 1st cycle, it shows that the composition of the SEI varies slightly. The amounts of Li_xSiO_y, ROCOOLi, ionic C-F and Li_xPO_yF_z appear to increase, and LiF and Li_xPF_y turn out to be less. This phenomenon can be ascribed to a couple of reasons: (1) Different reactions may take place over time due to the presence of the initial SEI stratum; (2) The SEI layer thickens slightly with fresh layers along cycling. Since XPS is surface sensitive, the SEI formed in later cycles is more visible.

4. Conclusions

In conclusion, the binder/carbon-free Si NP anode synthesized via

direct PECVD promises a particularly rapid and scalable synthesis method for Si anodes of Li ion batteries. The electrodes show high specific and areal capacity as well as cycling stability. The Si NP anode shows sufficient electronic conductivity facilitated by the lithiation of Si throughout the solid. Excellent cycling stability results from the in-situ formation of locally protective SEI on the clusters of the individual nanoparticles throughout the electrode; it apparently reinforces the cohesion of the clusters, the single particles as well as the entire electrode, while the electronic conduction throughout the electrode is maintained. Overall, this novel and binder/C-free Si anode exhibits unprecedented high areal capacity at high current rates and surprising resistance to electrode degradation. Using modified but large throughput solar photovoltaic production equipment the method also may provide a significant promise for the commercial large scale production of Si anodes for Li ion batteries.

Acknowledgement

This research is financially supported by A green Deal in Energy Materials (ADEM) grant funded by Dutch Ministry of Economic Affairs and ADEM industrial partners. H. W. Zandbergen and S. Basak would like to thank the European Research Council (ERC) project No. 267922 for the financial support.

Appendix A. Supporting information

Supplementary data associated with this article can be found in the online version at doi:10.1016/j.nanoen.2017.06.011.

References

- [1] S. Chu, A. Majumdar, *Nature* 488 (2012) 294–303.
- [2] B. Dunn, H. Kamath, J.-M. Tarascon, *Science* 334 (2011) 928–935.
- [3] M. Armand, J.M. Tarascon, *Nature* 451 (2008) 652–657.
- [4] Y. Sun, N. Liu, Y. Cui, *Nat. Energy* (2016) 16071.
- [5] J.M. Tarascon, M. Armand, *Nature* 414 (2001) 359–367.
- [6] M.N. Obrovac, L. Christensen, *Electrochem. Solid-State Lett.* 7 (2004) A93–A96.
- [7] D. Ma, Z. Cao, A. Hu, *Nano-Micro Lett.* 6 (2014) 347–358.
- [8] M. Ashuri, Q. He, L.L. Shaw, *Nanoscale* 8 (2016) 74–103.
- [9] X. Zuo, J. Zhu, P. Müller-Buschbaum, Y.-J. Cheng, *Nano Energy* 31 (2017) 113–143.
- [10] A.S. Arico, P. Bruce, B. Scrosati, J.-M. Tarascon, W. van Schalkwijk, *Nat. Mater.* 4 (2005) 366–377.
- [11] H. Wu, Y. Cui, *Nano Today* 7 (2012) 414–429.
- [12] X. Su, Q. Wu, J. Li, X. Xiao, A. Lott, W. Lu, B.W. Sheldon, J. Wu, *Adv. Energy Mater.* 4 (2014) 1300882.
- [13] C.K. Chan, H. Peng, G. Liu, K. McIlwrath, X.F. Zhang, R.A. Huggins, Y. Cui, *Nat. Nanotechnol.* 3 (2008) 31–35.
- [14] L.-F. Cui, R. Ruffo, C.K. Chan, H. Peng, Y. Cui, *Nano Lett.* 9 (2009) 491–495.
- [15] T. Song, J. Xia, J.-H. Lee, D.H. Lee, M.-S. Kwon, J.-M. Choi, J. Wu, S.K. Doo, H. Chang, W.I. Park, D.S. Zang, H. Kim, Y. Huang, K.-C. Hwang, J.A. Rogers, U. Paik, *Nano Lett.* 10 (2010) 1710–1716.
- [16] H. Wu, G. Chan, J.W. Choi, I. Ryu, Y. Yao, M.T. McDowell, S.W. Lee, A. Jackson, Y. Yang, L. Hu, Y. Cui, *Nat. Nanotechnol.* 7 (2012) 310–315.
- [17] H. Ma, F. Cheng, J.Y. Chen, J.Z. Zhao, C.S. Li, Z.L. Tao, J. Liang, *Adv. Mater.* 19 (2007) 4067–4070.
- [18] B. Liu, P. Soares, C. Checkles, Y. Zhao, G. Yu, *Nano Lett.* 13 (2013) 3414–3419.
- [19] B. Zhu, N. Liu, M. McDowell, Y. Jin, Y. Cui, J. Zhu, *Nano Energy* 13 (2015) 620–625.
- [20] X. Zhou, Y.-X. Yin, L.-J. Wan, Y.-G. Guo, *Adv. Energy Mater.* 2 (2012) 1086–1090.
- [21] K. Evanoff, A. Magasinski, J. Yang, G. Yushin, *Adv. Energy Mater.* 1 (2011) 495–498.
- [22] L. Xue, G. Xu, Y. Li, S. Li, K. Fu, Q. Shi, X. Zhang, *ACS Appl. Mater. Interfaces* 5 (2013) 21–25.
- [23] S.-M. Jang, J. Miyawaki, M. Tsuji, I. Mochida, S.-H. Yoon, *Carbon* 47 (2009) 3383–3391.
- [24] G. Liu, S. Xun, N. Vukmirovic, X. Song, P. Olalde-Velasco, H. Zheng, V.S. Battaglia, L. Wang, W. Yang, *Adv. Mater.* 23 (2011) 4679–4683.
- [25] C. Wang, H. Wu, Z. Chen, M.T. McDowell, Y. Cui, Z. Bao, *Nat. Chem.* 5 (2013) 1042–1048.
- [26] Q. Xiao, Y. Fan, X. Wang, R.A. Susantyo, Q. Zhang, *Energy Environ. Sci.* 7 (2014) 655–661.
- [27] H. Wu, G. Yu, L. Pan, N. Liu, M.T. McDowell, Z. Bao, Y. Cui, *Nat. Commun.* 4 (2013).
- [28] Y. Yao, M.T. McDowell, I. Ryu, H. Wu, N. Liu, L. Hu, W.D. Nix, Y. Cui, *Nano Lett.* 11 (2011) 2949–2954.
- [29] Z. Chen, C. Wang, J. Lopez, Z. Lu, Y. Cui, Z. Bao, *Adv. Energy Mater.* 5 (2015) 1614–6840.
- [30] I.H. Son, J. Hwan Park, S. Kwon, S. Park, M.H. Rummeli, A. Bachmatiuk, H.J. Song, J. Ku, J.W. Choi, J.-m. Choi, S.-G. Doo, H. Chang, *Nat. Commun.* 6 (2015).
- [31] D. Lin, Z. Lu, P.-C. Hsu, H.R. Lee, N. Liu, J. Zhao, H. Wang, C. Liu, Y. Cui, *Energy Environ. Sci.* 8 (2015) 2371–2376.
- [32] X. Li, M. Gu, S. Hu, R. Kennard, P. Yan, X. Chen, C. Wang, M.J. Sailor, J.-G. Zhang, J. Liu, *Nat. Commun.* 5 (2014).
- [33] N. Liu, Z. Lu, J. Zhao, M.T. McDowell, H.-W. Lee, W. Zhao, Y. Cui, *Nat. Nanotechnol.* 9 (2014) 187–192.
- [34] Y. Li, K. Yan, H.-W. Lee, Z. Lu, N. Liu, Y. Cui, *Nat. Energy* 1 (2016) 15029.
- [35] Q. Xu, J.Y. Li, J.K. Sun, Y.X. Yin, L.J. Wan, Y.G. Guo, *Adv. Energy Mater.* 6 (2016) 1601481.
- [36] M. Ko, S. Chae, J. Ma, N. Kim, H.-W. Lee, Y. Cui, J. Cho, *Nat. Energy* 1 (2016) 16113.
- [37] Y. Jin, S. Zhang, B. Zhu, Y. Tan, X. Hu, L. Zong, J. Zhu, *Nano Lett.* 15 (2015) 7742–7747.
- [38] L. Zong, B. Zhu, Z. Lu, Y. Tan, Y. Jin, N. Liu, Y. Hu, S. Gu, J. Zhu, Y. Cui, *Proc. Natl. Acad. Sci. USA* 112 (2015) 13473–13477.
- [39] L. Zong, Y. Jin, C. Liu, B. Zhu, X. Hu, Z. Lu, J. Zhu, *Nano Lett.* 16 (2016) 7210–7215.
- [40] G. Shoorideh, Y.S. Kim, Y.L. Joo, *Electrochim. Acta* 222 (2016) 946–955.
- [41] X. Hu, Y. Jin, B. Zhu, Y. Tan, S. Zhang, L. Zong, Z. Lu, J. Zhu, *ChemNanoMat* 2 (2016) 671–674.
- [42] L.-F. Cui, L. Hu, J.W. Choi, Y. Cui, *ACS Nano* 4 (2010) 3671–3678.
- [43] D.P. Wong, R. Suriyaprabha, R. Yuvakumar, V. Rajendran, Y.-T. Chen, B.-J. Hwang, L.-C. Chen, K.-H. Chen, *J. Mater. Chem. A* 2 (2014) 13437–13441.
- [44] D. Nan, Z.-H. Huang, R. Lv, Y. Lin, L. Yang, X. Yu, L. Ye, W. Shen, H. Sun, F. Kang, *J. Nanomater.* 2014 (2014) 10.
- [45] C. Li, C. Liu, W. Wang, J. Bell, Z. Mutlu, K. Ahmed, R. Ye, M. Ozkan, C.S. Ozkan, *Chem. Commun.* 52 (2016) 11398–11401.
- [46] L. Fei, S.H. Yoo, R.A.R. Villamayor, B.P. Williams, S.Y. Gong, S. Park, K. Shin, Y.L. Joo, *ACS Appl. Mater. Interfaces* 9 (2017) 9738–9746.
- [47] J. Graetz, C.C. Ahn, R. Yazami, B. Fultz, *Electrochem. Solid-State Lett.* 6 (2003) A194–A197.
- [48] H. Wolf, Z. Pajkic, T. Gerdes, M. Willert-Porada, *J. Power Sources* 190 (2009) 157–161.
- [49] H. Liu, L. Hu, Y.S. Meng, Q. Li, *Nanoscale* 5 (2013) 10376–10383.
- [50] E. Biserni, A. Scarpellini, A.L. Bassi, P. Bruno, Y. Zhou, M. Xie, *Nanotechnology* 27 (2016) 245401.
- [51] F. Cheng, Z. Tao, J. Liang, J. Chen, *Chem. Mater.* 20 (2008) 667–245681.
- [52] P. Singh, F.M. Mulder, A.M. Abdelkader, M. Wagemaker, *Adv. Energy Mater.* 3 (2013) 572–578.
- [53] B. Hoex, A.J.M. van Erven, R.C.M. Bosch, W.T.M. Stals, M.D. Bijkker, P.J. van den Oever, W.M.M. Kessels, M.C.M. van de Sanden, *Prog. Photovolt.: Res. Appl.* 13 (2005) 705–712.
- [54] I. Dogan, N.J. Kramer, R.H.J. Westermann, K. Dohnalova, A.H.M. Smets, M.A. Verheijen, T. Gregorkiewicz, M.C.M. v.d. Sanden, *J. Appl. Phys.* 113 (2013) 134306.
- [55] W. Wan, Q. Zhang, Y. Cui, E. Wang, *J. Phys. Condens. Matter* 22 (2010) 415501.
- [56] M.T. McDowell, Y. Cui, *Adv. Energy Mater.* 1 (2011) 894–900.
- [57] E. Pollak, G. Salitra, V. Baranchugov, D. Aurbach, *J. Phys. Chem. C* 111 (2007) 11437–11444.
- [58] R. Ruffo, S.S. Hong, C.K. Chan, R.A. Huggins, Y. Cui, *J. Phys. Chem. C* 113 (2009) 11390–11398.
- [59] J. Guo, A. Sun, X. Chen, C. Wang, A. Manivannan, *Electrochim. Acta* 56 (2011) 3981–3987.
- [60] M.B. Pinson, M.Z. Bazant, *J. Electrochem. Soc.* 160 (2013) A243–A250.
- [61] V. Etacheri, O. Haik, Y. Goffer, G.A. Roberts, I.C. Stefan, R. Fasching, D. Aurbach, *Langmuir* 28 (2012) 965–976.
- [62] Y.-M. Lin, K.C. Klavetter, P.R. Abel, N.C. Davy, J.L. Snider, A. Heller, C.B. Mullins, *Chem. Commun.* 48 (2012) 7268–7270.
- [63] K. Schroder, J. Alvarado, T.A. Yersak, J. Li, N. Dudney, L.J. Webb, Y.S. Meng, K.J. Stevenson, *Chem. Mater.* 27 (2015) 5531–5542.
- [64] W.-S. Chang, C.-M. Park, J.-H. Kim, Y.-U. Kim, G. Jeong, H.-J. Sohn, *Energy Environ. Sci.* 5 (2012) 6895–6899.
- [65] N. Yan, F. Wang, H. Zhong, Y. Li, Y. Wang, L. Hu, Q. Chen, *Sci. Rep.* 3 (2013) 1568.
- [66] X. Hu, K. Zhang, L. Cong, F. Cheng, J. Chen, *Chem. Commun.* 51 (2015) 15827.



Yaolin Xu received his B.Sc. in physics in Renmin University of China in 2011, and obtained his M.Sc. in Sustainable Energy of Technology at Delft University of Technology in 2013. He is currently a Ph.D. student in Department of Chemical Engineering at Delft University of Technology and his research is mainly focused on the materials for Li- and Na-ion batteries.



Ellie Swaans received her M.Sc. degree in chemical engineering from Technical University Eindhoven in 1998. She is currently senior process development engineer at Meyer Burger Netherlands, where she is working on the development of production processes regarding Silicon based anodes for Li-ion batteries.



Bo Peng received his B.Sc. degree in physics from Renmin University of China in 2011. He is currently a Ph.D. student in Department of Physics at Renmin University of China. His research interest mainly focuses on the anode materials for Li- and Na-ion batteries.



Sibò Chen received her Bachelor of Engineering (B.E.) in environmental engineering in Nanjing Normal University in 2013. She accomplished her M.Sc. study in Sustainable Energy Technology in Delft University of Technology in 2015 and is now working as a process engineering in Meyer Burger. Her research interests include plasma enhanced chemical vapour deposition (PECVD) and Li-ion batteries.



Prof. Dr. Henny W. Zandbergen is a professor in Kavli Institute of Nanoscience Delft at Delft University of Technology. He received his Ph.D. degree in solid-state chemistry from Leiden University and had started working in the field of TEM from 1984. His research interests are mainly directed towards the development of quantitative electron diffraction and in-situ TEM and his interest in developing in-situ TEM has led to the fabrication of dedicated sample holders.



Shibabrata Basak received his M.Tech. in solid state physics from IIT Kharagpur in 2010. He is currently a Ph.D. student in Kavli Institute of Nanoscience at Delft University of Technology. His research interest mainly focuses on understanding the fundamental of Li-ion batteries using electron microscopy including in-situ TEM study.



Dr. Dana M. Borsa is the Research Manager of the Thin Film Coating and Projects Business Unit at Meyer Burger (Netherlands) B.V. responsible for all process and application developments. Her Ph.D. in physics from the Rijks Universiteit Groningen was focused on the growth and characterization of nitride-based thin films and multi-layers. After some years of research on switchable mirrors and hydrogen storage materials at Vrije Universiteit Amsterdam she moved to ECN and worked on high efficiency solar cell concepts before joining OTB Solar (currently Meyer Burger (Netherlands) B.V.) in 2009.



Peter-Paul R.M.L. Harks received his M.Sc. degree in physics from Utrecht University in the Netherlands. He is currently working as a Ph.D. student in Department of Chemical Engineering at Delft University of Technology. In his research he mainly focuses on high-energy density electrode materials for Li- and Na-ion batteries.



Prof. Dr. Fokko M. Mulder is professor of materials for integrated energy systems in Faculty of Applied Sciences at Delft University of Technology. During his Ph.D. in physics at Leiden University he published on electronic properties of metal nanoparticles and on permanent magnetic materials. Currently his research is focused on energy storage and conversion materials including Li- and Na-ion batteries and Hydrogen storage and production.